arXiv:astro-ph/0101335v1 18 Jan 2001

A Comprehensive Statistical Analysis of the Gas Distribution in Lyman-limit and Damped Lyman-α Absorption Systems

Rino Bandiera

Osservatorio Astrofisico di Arcetri, Largo E.Fermi, 5, 50125 - Italy

bandiera@arcetri.astro.it

and

Edvige Corbelli

Osservatorio Astrofisico di Arcetri, Largo E.Fermi, 5, 50125 - Italy

edvige@arcetri.astro.it

ABSTRACT

In this paper we show how to use data on Lyman-limit and Damped Lyman-α absorption systems to derive the hydrogen ionization fractions and the distribution of the face-on total gas column density. We consider axially symmetric, randomly oriented absorbers, ionized by an external background radiation field in order to relate the face-on total gas distribution to that of the neutral hydrogen observed along the line of sight. We devise a statistical procedure based on the Maximum Likelihood criterion, that is able to treat simultaneously data coming from different surveys and statistically recovers the "true" column densities in the presence of large uncertainties: this is especially important for Lyman-limit systems which leave an unmeasurable residual flux at wavelengths shorter than the Lyman break. We make use of simulated data to look for possible observational biases and extensively test our procedure. For a large statistical sample of real data in the redshift range [1.75,3.25] (collected from all published surveys) our Maximum Likelihood procedure gives a power-law slope for the total hydrogen distribution of -2.7. All together Lyman-limit systems therefore contain more gas than Damped Lyman-α systems. Analysis of data at other redshifts shows that more observations are needed to reach a compelling evidence for a cosmological evolution of the slope of the gas distribution.

Subject headings: methods: statistical — quasars: absorption lines — catalogs

1. Introduction

Absorption features in quasar spectra represent a powerful tool to investigate the formation and evolution of gaseous structures in the early Universe (Rauch 1998, and references therein), the efficiency of processes such as merging (Kauffmann 1996), gas depletion due to star formation (Wolfe et al. 1995; Storrie-Lombardi and Wolfe 2000), and ionization by the ultraviolet background radiation field (Weinberg et al. 1997; Savaglio et al. 1997). Also the level of cloud clustering may be investigated analyzing absorption spectra (Cristiani et al. 1997). Lyman-limit absorption systems (hereafter LLS) are cosmological structures which contain enough neutral hydrogen to absorb Lyman continuum photons and produce a break in the QSO continuum flux level. This feature is detectable in moderate-resolution spectra whenever the opacity to Lyman continuum photons satisfies the condition $\tau_{LL} \gtrsim 1$, equivalent to a neutral hydrogen column density $N_{\rm HI} \geq 1.6 \times 10^{17}\,{\rm cm}^{-2}$. The column density of LLS can be determined whenever a residual flux beyond the Lyman break is detectable. Systems with $N_{\rm HI} \gtrsim 5 \times 10^{19}\,{\rm cm}^{-2}$ are also visible in moderate-resolution spectra since they give rise to Damped Lyman-α absorption lines with a reference frame equivalent width $\geq 5\,$Å. In this paper we shall refer to these as Damped Lyman-α absorption systems (hereafter DLS). The HI column density of absorbers is usually very poorly determined observationally when $5 \times 10^{17} < N_{\rm HI} < 5 \times 10^{19}\,{\rm cm}^{-2}$ since the Lyman break is saturated, while the Lyman-α absorption line is not yet damped. Previous studies of absorbers with poorly determined column densities have been carried out using a coarse binning in $N_{\rm HI}$. But a coarse binning suffers by statistical problems, related to the fact that different choices of binning may lead to different results (e.g. Stengler-Larrea et al. (1995) for problems related to redshift binning), as well as by some negative consequences on the physical description, because it does not differentiate HI column densities which correspond to different ionization conditions. This is particularly important for $10^{17} < N_{\rm HI} < 10^{20}\,{\rm cm}^{-2}$ since in this range a smoothly varying total gas column density distribution leads to a rapidly varying HI column density distribution due to the rapid change of the H ionization fraction (Corbelli et al. 2000, hereafter Paper I).

To tackle this problem, we have collected data on LLS and DLS from all the available literature and perform a comprehensive statistical analysis, based on a Maximum Likelihood procedure, which allows a joined fit of observations with different $N_{\rm HI}$ sensitivities and uncertainties, with different ionization conditions and at different redshifts.

The outline of this paper is the following: in Section 2 we discuss how the observed HI column density distribution is related to the total hydrogen distribution for face-on absorbers. A set of analytical solutions for the cross section of non-spherical absorbers, randomly oriented in space, is reported in Appendix A. Section 3 contains a description of the database.

Section 4 details the statistical algorithm that we use to best fit the HI column density distribution of absorbers. Section 4 also summarizes results relative to our database. In Section 5 we perform realistic simulations of the data, which are used to test the effectiveness and the robustness of the statistical algorithm.

2. Column densities relationships

One physically meaningful quantity for investigating the formation and evolution of gas condensations is the distribution of their gaseous mass. However observations measure only the distribution of the neutral hydrogen column density along the line of sight, which may present a rather complex behavior even if the face-on total column density distribution is a power law. In this section we show how to transform one distribution into the other. The relationship between the total and the neutral column density has been investigated in detail in Paper I. Here we focus on the effect of randomly oriented absorbers which are either flat or of ellipsoidal shape.

2.1. From the total to the neutral column density distribution

We show first how a face-on total hydrogen column density distribution $g_\perp(N_{\rm H\perp})$ translates into a face-on neutral hydrogen distribution $f_\perp(N_{\rm HI\perp})$. For a generic relationship $N_{\rm H\perp}\left(N_{\rm HI\perp}\right)$ one can write:

$$f_\perp\left(N_{\rm HI\perp}\right) = g_\perp\left(N_{\rm H\perp}\right)\frac{dN_{\rm H\perp}}{dN_{\rm HI\perp}}. \tag{1}$$

If $g_\perp$ is a pure power-law:

$$g_\perp\left(N_{\rm H\perp}\right) = KN_{\rm H\perp}^{-\alpha} \tag{2}$$

$f_\perp\left(N_{\rm HI\perp}\right)$ is also a power law when $N_{\rm H\perp} = QN_{\rm HI\perp}^{\beta}$:

$$f_\perp\left(N_{\rm HI\perp}\right) = \beta KQ^{-(\alpha-1)}N_{\rm HI\perp}^{-\xi}, \tag{3}$$

with $\xi = 1+\beta(\alpha-1)$. For $\beta \leq 1$ (an ionization fraction monotonically decreasing with $N_{\rm H\perp}$) and $\alpha > 1$, $f_\perp\left(N_{\rm HI\perp}\right)$ is always shallower than $g_\perp\left(N_{\rm H\perp}\right)$.

For a generic $N_{\rm H\perp}\left(N_{\rm HI\perp}\right)$ relationship, $f_\perp(N_{\rm HI\perp})$ is not tied to a power law. For example when there is a sharp break in the slope of $N_{\rm H\perp}\left(N_{\rm HI\perp}\right)$ at N_b, $f_\perp$ is not continuous at N_b, being larger on the side where its slope is steeper:

$$f_\perp\left(N_{\rm HI\perp}\right) = K'\Big(\ \left(\xi_1-1\right)\left(N_{\rm HI\perp}/N_b\right)^{-\xi_1}\Theta\left(N_b - N_{\rm HI\perp}\right)\ \ +$$

$$(\xi_2 - 1)\,(N_{\rm HI\perp}/N_b)^{-\xi_2}\Theta\,(N_{\rm HI\perp} - N_b)\,\Big), \tag{4}$$

where $\Theta(x)$ is the Heaviside step function.

Similarly we can consider multiple breaks: for example if $N_{\rm HI\perp} = N_{\rm H\perp}$ for large $N_{\rm HI\perp}$ and $N_{\rm HI\perp} = \epsilon N_{\rm H\perp}$ for small $N_{\rm HI\perp}$ (as for a constant ionization fraction), $f_\perp$ follows a power law with index $-\alpha$ in both regions, but the low-column density distribution is shifted by a factor $\epsilon^{\alpha-1}$ with respect to the extrapolation of the high-column density one.

2.2. Orientation-averaged differential cross section

In this section we consider the effects of the random orientation of non-spherical absorbers on the observed column density distribution. We derive a simple analytic solution for "infinitely thin homogeneous slabs", namely those whose thickness ($2h$) is much smaller than their radial extension ($2R$), and whose face-on gas column density is constant. We then test a simple approximation for treating "finite thickness slabs", using the exact solution for homogeneous ellipsoids, given in Appendix A.

Let $\sigma(N_{\rm HI}, \mu)$ be the differential cross section of an absorber, whose symmetry axis is tilted by an angle θ with respect to the line of sight. Its differential cross section, averaged over orientations, is:

$$\hat{\sigma}(N_{\rm HI}) = \frac{1}{2}\int_{-1}^{1} \sigma(N_{\rm HI}, \mu)\; d\mu \tag{5}$$

(where we have defined $\mu \equiv \cos\theta$). For infinitely thin slabs of surface area A and face-on column density $N_{\rm HI\perp}$, the averaged cross section reads:

$$\hat{\sigma}(N_{\rm HI}) = \frac{1}{2}\int_{-1}^{1} A\,|\mu|\,\delta(N_{\rm HI} - N_{\rm HI\perp}/|\mu|)\; d\mu = \frac{A N_{\rm HI\perp}^2}{N_{\rm HI}^3}\,\Theta\,(N_{\rm HI} - N_{\rm HI\perp})\,, \tag{6}$$

where $\delta(x)$ is the Dirac distribution. Therefore the averaged cross section vanishes for $N_{\rm HI} < N_{\rm HI\perp}$, and is proportional to $N_{\rm HI}^{-3}$ for $N_{\rm HI} > N_{\rm HI\perp}$.

For absorbers of finite thickness the exact behavior of $\hat{\sigma}$ depends on their detailed shape, but the following approximate formula holds:

$$\hat{\sigma}(N_{\rm HI}) = \frac{A N_{\rm HI\perp}^2}{N_{\rm HI}^3}\,\Theta\,(N_{\rm HI} - N_{\rm HI\perp})\;\Theta\,(N_{\rm HI\perp} R/h - N_{\rm HI})\,. \tag{7}$$

It is shown in Appendix A that the accuracy of Eq. (7) decreases as h/R grows larger. When $h \sim R$, $\hat{\sigma}$ for ellipsoidal absorbers differs noticeably from Eq. (7); but, once Eq. (7) is convolved with realistic $f_\perp$ distributions, results keep close to the exact ones.

2.3. From the face-on to the line of sight $N_{\rm HI}$ distribution

The line of sight $N_{\rm HI}$ distribution, $f(N_{\rm HI})$, can be written as:

$$f\left(N_{\rm HI}\right) = \int \frac{\hat{\sigma}(N_{\rm HI})}{A} f_{\perp}(N_{\rm HI\perp})\ dN_{\rm HI\perp}, \tag{8}$$

which, using Eq. (7), gives:

$$f\left(N_{\rm HI}\right) = \frac{1}{N_{\rm HI}^3} \int_{N_{\rm HI}h/R}^{N_{\rm HI}} N_{\rm HI\perp}^2 f_{\perp}(N_{\rm HI\perp})\ dN_{\rm HI\perp}. \tag{9}$$

This equation shows that $f(N_{\rm HI})$ is sensitive to the values of $f_{\perp}$ over the whole range $[N_{\rm HI}\,h/R, N_{\rm HI}]$ (i.e. $[0, N_{\rm HI}]$ for infinitely thin slabs).

If there is a single break in $f_{\perp}$, as given by Eq. (4), the corresponding $f(N_{\rm HI})$ is:

$$f\left(N_{\rm HI}\right) = \frac{K}{N_{\rm HI}^3}\Bigg(\frac{\xi_1 - 1}{3-\xi_1} N_b^{\xi_1} \left(\min\left(N_{\rm HI}, N_b\right)^{3-\xi_1} - \min\left(N_{\rm HI}h/R, N_b\right)^{3-\xi_1}\right) + \frac{\xi_2 - 1}{3-\xi_2} N_b^{\xi_2} \left(\max\left(N_{\rm HI}, N_b\right)^{3-\xi_2} - \max\left(N_{\rm HI}h/R, N_b\right)^{3-\xi_2}\right)\Bigg). \tag{10}$$

For $N_{\rm HI} < N_b$ and for $N_b R/h < N_{\rm HI}$, f follows power laws with indices $-\xi_1$ and $-\xi_2$ respectively. In the intermediate $N_{\rm HI}$ range the behavior of f is more complex: if $f_{\perp}$ is steeper at $N_{\rm HI} < N_b$, its slope approaches -3 for $N_b < N_{\rm HI} \ll N_b R/h$ while it bends to connect to the power-law regime at $N_{\rm HI} > N_b R/h$; in the opposite case f suddenly rises for $N_{\rm HI} > N_b$, and then smoothly connects with the high column density power-law branch.

Fig. 1 shows qualitatively the features present in $f(N_{\rm HI})$ for a realistic $N_{\rm H\perp}(N_{\rm HI\perp})$ relationship (see Paper I): $N_{\rm H\perp} \propto N_{\rm HI\perp}^{\beta}$ for $N_{b1} \leq N_{\rm HI\perp} \leq N_{b2}$, $N_{\rm H\perp} \propto N_{\rm HI\perp}$ elsewhere. We choose $\alpha = 1.5$, $h/R = 0.1$, $N_{b1} = 10^{17}\,{\rm cm}^{-2}$, $N_{b2} = 10^{20}\,{\rm cm}^{-2}$, and $\beta = 0.001$ to emphasize the various regimes described above. Note that $f(N_{\rm HI})$ at low column densities is lower by a factor $(N_{b1}/N_{b2})^{(1-\beta)(\alpha-1)}$ with respect to the extrapolation of the distribution at high column densities (dashed line). At intermediate column densities a dip in the distribution appears, approaching a -3 slope towards the low column density side.

3. DLS&LLS surveys and our data sample

In this section we show which information should be extracted from the large number of DLS&LLS surveys available in order to build up a homogeneous database for a global statistical approach.

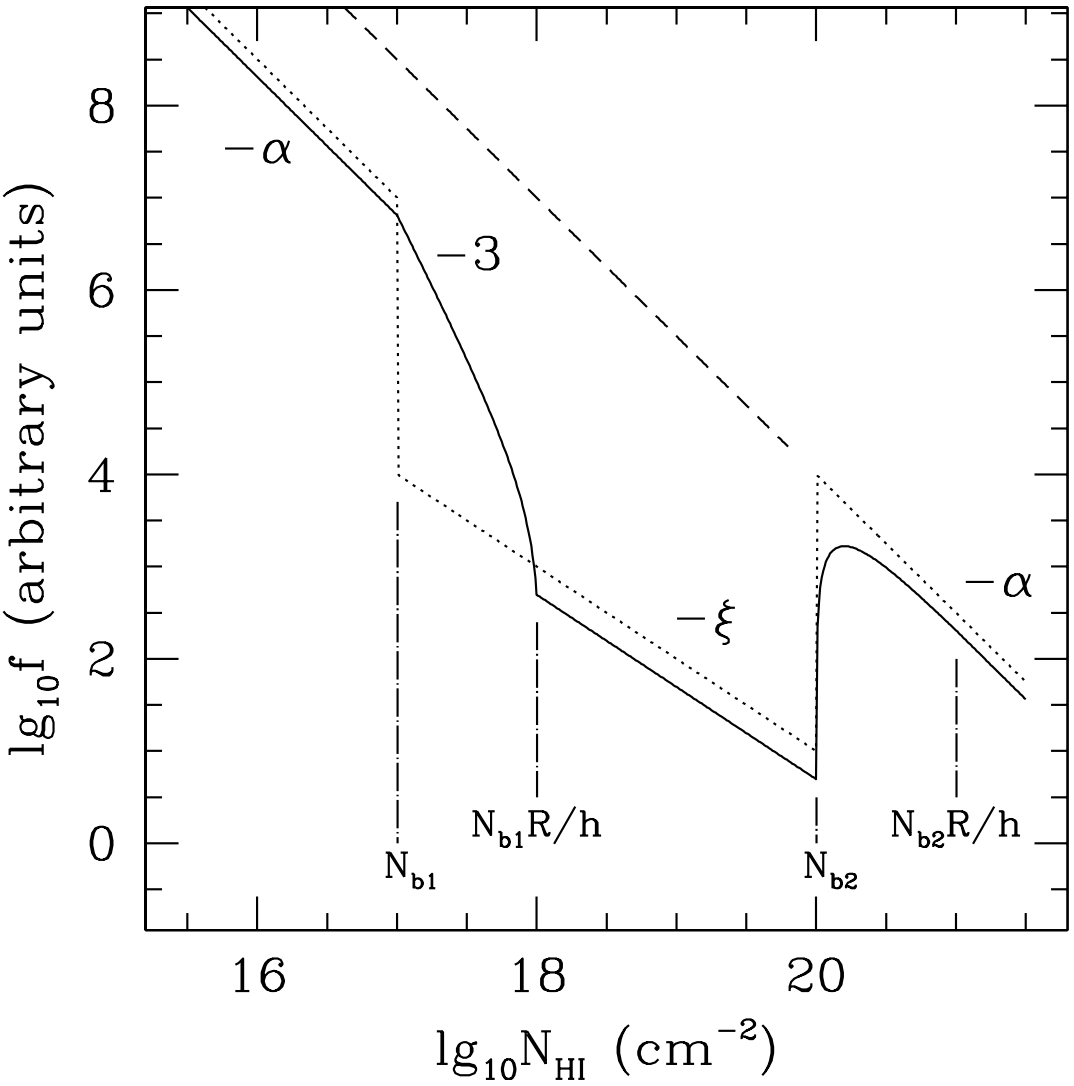

Fig. 1.— For a given face-on $N_{\rm HI}$ distribution (dotted line) we show the projected distribution $f(N_{\rm HI})$ (solid line). The original face-on total gas distribution is also plotted (dashed line). Power-law indices in regions where $f(N_{\rm HI})$ approaches a power law are indicated. We have used a realistic relationship between $N_{\rm H\perp}$ and $N_{\rm HI\perp}$ given explicitly in the text.

In a LLS the value of $N_{\rm HI}$ can be determined from the ratio between I, the residual Lyman continuum flux on the blue side of the break, and I_0, the unabsorbed continuum flux:

$$N_{\rm HI} = 1.6 \times 10^{17} \tau_{LL} \, {\rm cm}^{-2} = 1.6 \times 10^{17} \ln (I_0/I) \ {\rm cm}^{-2}. \quad (11)$$

If the residual flux I is too small to be measured, only a lower limit to $N_{\rm HI}$ can be derived: this usually happens for $\tau_{LL} \gtrsim 3$. Since there are measurements sensitive to Lyman continuum optical depths as small as 0.4, we include in our database all LLS surveys which are sensitive to $N_{\rm HI} \geq 10^{16.81} \, {\rm cm}^{-2}$.

We include in the compilation all available searches for absorption lines with a rest frame equivalent width $W \geq 5 \, {\rm Å}$, for which $N_{\rm HI}$ can be estimated from:

$$N_{\rm HI} = 1.88 \times 10^{18} \, W^2 \, {\rm cm}^{-2}. \quad (12)$$

A complication comes from the fact that spurious lines with large equivalent width may result from a blending of weaker lines with metal line systems or Lyman-α forest lines. Only some surveys have sufficient spectral resolution to test, by fitting a Voigt profile, whether lines with $W \geq 5 \, {\rm Å}$ are really damped. In our database we include both the column density value determined directly from Eq. (12) and that derived from the Voigt profile fit, whenever this is available. By comparing these two values we find that there is a bias in the $N_{\rm HI}$ values estimated from the equivalent width, and derive the following statistical correction:

$$\lg_{10} N_{{\rm HI},corr} = 6.261 + 0.705 \lg_{10} N_{{\rm HI},W}. \quad (13)$$

We apply this correction to all absorption lines for which only the W value is available. If only a lower limit to τ_{LL} can be derived from the Lyman continuum absorption, searches for the corresponding damped Lyman-α line can be used to establish a value or an upper limit to the HI column density. If the corresponding Lyman-α absorption line has not been searched for, we take an upper limit of $5 \times 10^{21} \, {\rm cm}^{-2}$, which is the highest measured value of $N_{\rm HI}$ in our database.

Unfortunately upper limits to saturated LLS leave large uncertainties in the column density range $5 \times 10^{17} \lesssim N_{\rm HI} \lesssim 5 \times 10^{19} \, {\rm cm}^{-2}$, where theoretical predictions are very sensitive to the detailed shape of the $N_{\rm H\perp}(N_{\rm HI\perp})$ relationship. Hence it is essential to find a correct statistical approach for evaluating the $N_{\rm HI}$ distribution in the presence of large uncertainties to determine the ionization conditions of the gas as well as the total gas column density distribution in LLS and DLS.

We have collected data from the following references: Tytler (1982); Bechtold et al. (1984); Wolfe et al. (1986); Tytler (1987); Lanzetta (1988); Sargent, Steidel and Boksenberg

(1989); Turnshek et al. (1989); Lanzetta (1991); Lanzetta et al. (1991); Courvoisier and Paltani (1992); Bahcall et al. (1993); Storrie-Lombardi et al. (1994); Lanzetta et al. (1995); Stengler-Larrea et al. (1995); Wolfe et al. (1995); Storrie-Lombardi et al. (1996); Jannuzi et al. (1998); Storrie-Lombardi and Wolfe (2000). In order to ensure an accurate estimate of the coverage of the survey we have excluded from the compilation the full spectrum or part of it whenever the continuum was visually found to be very noisy or non-uniform (e.g. some spectrum edges where the flux is below the 2-σ level in Lanzetta et al. (1995) or the objects 1130-106Y, PKS1206+459, MC1215+113 in Bahcall et al. (1993)). The final number of directions i.e. of QSOs included is 661. We have decided to split each direction in parts (hereafter called "paths") such that each path is defined by homogeneous search parameters and contains at most one detection. In other words one direction may correspond to more than one path if different sensitivities are used, or if more than one absorber is present along the line of sight. Our database is available in electronic form upon request to the authors. Parameters contained in the data table can be divided into two groups: those describing the search, and those related to the detection.

The main parameters associated with the search coverage are: *(i)* the redshift path limits, i.e. the upper and lower redshift for one direction in space observed with a given sensitivity; *(ii)* the sensitivity, specified by the threshold above which $N_{\rm HI}$ was detectable.

For each direction the upper redshift was set to $5000\,{\rm km\,s^{-1}}$ less than the QSO redshift, whenever the spectral coverage extends beyond it. We have usually taken as the lowest redshift that given by the observers. This does not coincide with the spectral coverage boundary in the presence of "shadowing effect". The "shadowing effect" intervenes whenever the continuum flux, absorbed by a LLS at z_*, gets below detectability: in this case the lower limit of the path has been set to z_*. If no DLS searches have been performed no further paths are appended along that direction; otherwise, due to the different frequency of the Lyman-α line respect to the H ionization threshold, further paths are considered between z_* and the Lyman-α shadowing redshift ($z = 0.75z_* - 0.25$). The lowest redshift of the LLS search in the absence of shadowing is reported in the database as well, since in Section 5 it will be used for simulating data samples. The sensitivity for a Lyman-limit search depends on the minimum opacity detectable in the survey: typically $\tau_{LL} = 0.4$, 1.0 or 1.5, corresponding to column density thresholds $\lg_{10} N_{th}$ =16.81, 17.20 and 17.38 respectively. We have set to 0.4 the minimum detectable τ_{LL} for observations listed in Bahcall et al. (1993) and Tytler (1987); we have instead set to 1.0 the threshold for all the observations listed in Lanzetta (1991) and Sargent, Steidel and Boksenberg (1989) which were revised by Stengler-Larrea et al. (1995). For absorption line searches with rest frame equivalent width $W \geq 5\,$Å the sensitivity of the path was set to $\lg_{10} N_{\rm HI} = 20.13$ (since we have applied the correction given in Eq. (13)). If both LLS and DLS searches were performed on the same path the threshold

of the path was set to the lowest of the two, except in the presence of shadowing effects.

The parameters associated with the detections are: *(i)* the redshift of the detected absorber; *(ii)* the decimal logarithm of the estimated HI column density of the absorber along the line of sight ($\lg_{10} N_{\rm HI}$); *(iii)* the minimum and the maximum allowed values for $\lg_{10} N_{\rm HI}$; *(iv)* the Voigt correction factors.

When $\lg_{10} N_{\rm HI}$ could not be determined from τ_{LL} or W measures, but only limits for it are available, we have reported as $\lg_{10} N_{\rm HI}$ the arithmetic mean between the minimum and maximum allowed values. When instead the value of $\lg_{10} N_{\rm HI}$ could be directly determined we have estimated the minimum and maximum allowed values by assuming a standard spread. In the case of non-saturated LLS we have used a spread of ± 0.2 in decimal logarithm, except for the cases listed in Jannuzi et al. (1998) for which we took the uncertainties quoted by the authors. In the case of DLS we have used again a spread of ± 0.2 when the line profile has been resolved and the Voigt profile has been fitted; otherwise we have used ± 0.4. The uncertainties in $\lg_{10} N_{\rm HI}$ that we quote are usually larger than those that can be directly derived from uncertainties on either τ_{LL} or W. This is because there are other sources of errors, such as the determination of the level of the continuum (which affects both W and τ_{LL} estimates), or the possible blending with other small absorption lines. The Voigt correction factors are the differences between the $\lg_{10} N_{\rm HI}$ values derived from the Voigt-profile fit and those from W (Eq. (12)).

Two further columns contain flags, which are different from 0 whenever LLS and DLS searches respectively have been performed on a given path. A value of -1 implies that no systems were found, a value of 1 means that the column density estimate is quite accurate, 2 that it is less accurate and 3 that it is very uncertain, as for DLS declared "non damped". In this last case the column density value for the DLS has been set to zero, or used as an upper limit if saturated LLS are detected at the same redshift.

The coverage of the whole sample, with and without shadowing, for various search sensitivities is shown in Fig. 2, where the inhomogeneity of the actual coverage is evident.

4. Statistical Analysis of the Data

Various authors have analyzed Lyman-α absorbers data to determine the $N_{\rm HI}$ distribution and/or its evolution with time. Nevertheless no statistical analysis of the $N_{\rm HI}$ distribution in LLS and DLS has been attempted so far using all available data and without a pre-defined coarse binning. In the following we show how to perform a global unbinned statistical analysis of heterogeneous data.

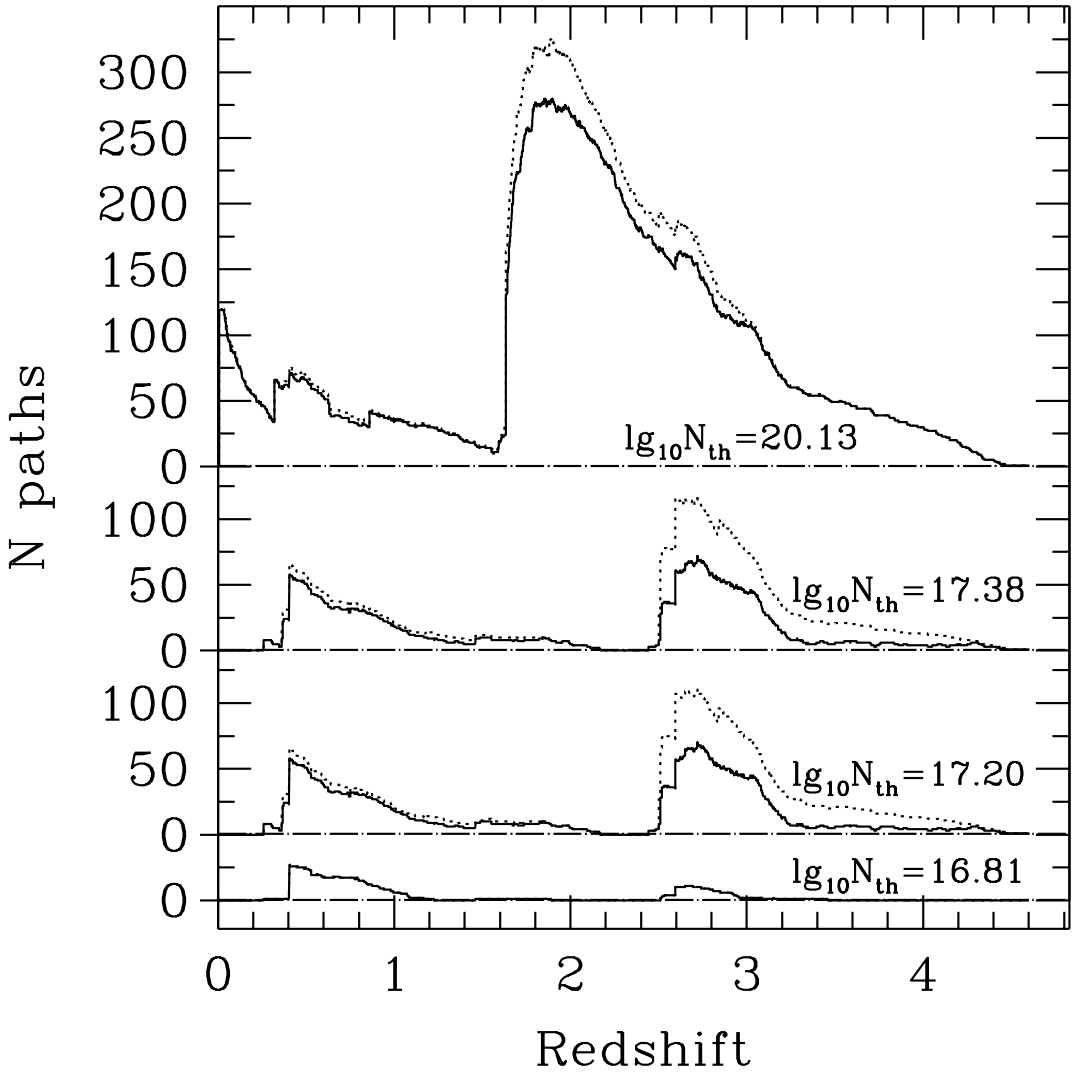

Fig. 2.— The redshift coverage of our sample for the various thresholds in column density ($\lg_{10} N_{th}$ =16.81, 17.20, 17.38 and 20.13). The continuum lines refer to the actual (shadowed) coverage, while the dotted ones refer to the case without shadowing.

4.1. Maximum Likelihood Analysis

Our approach for estimating the $N_{\rm HI}$ distribution is similar to the Maximum Likelihood analysis used by Storrie-Lombardi et al. (1996), with the following two improvements: *(i)* we use a generic (not just a pure power-law) distribution for $N_{\rm HI}$; *(ii)* we take into account uncertainties in the $N_{\rm HI}$ measurements. In order to simplify the notation we shall use the symbol N instead of $N_{\rm HI}$ in this section as well as in Section 4.2.

Let $f(N,z)$ be the distribution of column density N at redshift z. The average number of detections along a given direction is $f(N,z)\,\delta v$, where $\delta v = \delta N \delta z$ is the area of an infinitesimal cell in the N–z plane. For infinitesimal cells the probability of having more than one detection in the same cell is negligible. The probabilities of having zero or one detection in a given cell are respectively:

$$P_0(N,z) = \exp\left(-f\,\delta v\right); \qquad P_1(N,z) = (f\delta v)\exp\left(-f\,\delta v\right). \tag{14}$$

The likelihood for a given data set is the product of the probabilities over "all" cells in the N–z plane and over all directions in space. This product can be separated into two factors, one relative to the "empty" cells, and the other to the "full" cells:

$$\mathcal{L}_o = \prod_{i=\rm all} P_i = \prod_{i=\rm empty} P_{0,i} \prod_{j=\rm full} P_{1,j} = \prod_{i=\rm all} \exp\left(f_i \delta v\right) \prod_{j=\rm full} \left(f_j \delta v\right). \tag{15}$$

We know the total number of full cells (i.e. the number of detections, hereafter p) but we might not be able to position the detections into specific cells in the N–z plane due to the large uncertainties of N. For instance, if a detection has N_j in the range $[N_{min,j}, N_{max,j}]$, the absorber is in one of the cells of this N range, but we don't know in which one: the probability for this event is the sum of probabilities relative to the cells (the same considerations would apply to errors in z if redshifts are not well determined). In the limit of small cell sizes, the sum is then approximated by an integral of f over the allowed range of N, and the logarithmic value of $\mathcal{L}_o$ reads:

$$\ln \mathcal{L}_o = -\int w(N,z) f(N,z)\, dN dz + \sum_{j=1}^{p} \ln\left(\int_{N_{min,j}}^{N_{max,j}} f(N,z_j)\, dN\, \delta z\right), \tag{16}$$

where $w(N,z)$ is the number of different paths at a given z with a column density threshold smaller than N. The first term in Eq. (16) is related only to the parameters of the search, and can be evaluated using the normalization condition for f:

$$\int w(N,z) f(N,z)\, dN dz = p. \tag{17}$$

We can rewrite Eq. (16) using the above normalization condition:

$$\ln \mathcal{L}_o = p\,(\ln(\delta z) - 1) + \sum_{j=1}^{p} \ln\left(\int_{N_{min,j}}^{N_{max,j}} f(N, z_j)\, dN\right). \quad (18)$$

If column densities have been measured with a rather small uncertainty for a number p_1 of absorbers, Eq. (18) can be approximated as:

$$\ln \mathcal{L}_o = p\,(\ln(\delta z) - 1) + \sum_{j=1}^{p_1} \ln(\delta N_j) + \sum_{j=1}^{p_1} \ln\left(f(N_j, z_j)\right) + \sum_{j=p_1+1}^{p} \ln\left(\int_{N_{min,j}}^{N_{max,j}} f(N, z_j)\, dN\right), \quad (19)$$

which allows a faster numerical computation. The terms with δN_j and δz are constant and can be neglected while searching for the maximum value of $\mathcal{L}_o$. The limiting case $p_1 = p$ reduces Eq. (19) to the formula in Storrie-Lombardi et al. (1996).

4.2. The fit goodness and the true column density distribution

The Maximum Likelihood analysis does not contain any statistical test on the goodness of the "best" solution for f, since the absolute value of $\mathcal{L}_o$ is undetermined by a constant factor. Such a test can be done for example by comparing the theoretical versus the observational cumulative function. For large uncertainties of the column density values, this comparison requires a reasonable guess at the "true" value of N for each individual detection. A "reasonable" guess does not necessarily mean that each N value should reproduce the true one but that their overall distribution cannot be distinguished from the original one. We will show how to find this "reasonable" guess in the presence of large measurement uncertainties in N in order to avoid the use of a coarse binning.

For a given absorber j the probability of having a true column density smaller than N in the allowed range $[N_{min,j}, N_{max,j}]$ is:

$$R(N, j) = \int_{N_{min,j}}^{N} f(N', z_j)\, dN' \Big/ \int_{N_{min,j}}^{N_{max,j}} f(N', z_j)\, dN'. \quad (20)$$

R_j behave as random quantities and should have a uniform distribution in the interval $[0, 1]$, independently of the shape of the distribution function f.

The probability of having a detection with column density smaller than N in the overall N range, is:

$$C(N, j) = \int_{N_{th,min}}^{N} w(N', z_j) f(N', z_j)\, dN' \Big/ \int_{N_{th,min}}^{\infty} w(N', z_j) f(N', z_j)\, dN'. \quad (21)$$

The distribution of C_j should also be uniform in the interval $[0, 1]$, and is equivalent to the N cumulative distribution for a narrow range of redshift.

For a sample of x_j (sorted for increasing x_j values, with $0 \leq x_j \leq 1$ and $1 \leq j \leq p$) the cumulative distribution can be written as:

$$S(x) = \begin{cases} 0, & x < x_1 \\ j/p, & x_j \leq x < x_{j+1} \\ 1, & x_p \leq x. \end{cases} \tag{22}$$

The conventional way to test whether a given a distribution is compatible with the uniform one is to use the Kolmogorov-Smirnov test on the maximum deviation between the two cumulative functions:

$$D = \max_{0 \leq x \leq 1} |S(x) - x| \,; \tag{23}$$

the significance of D being given by the function $Q_{KS}(\sqrt{p}D)$ (Kendall and Stuart 1967).

However if the maximum discrepancy between the two distributions originates from some bias, the Kolmogorov-Smirnov test becomes completely insensitive to the overall match. Such effect is reduced if instead of D we use the quantity U:

$$U^2 = p \int_0^1 \left(S(x) - x - \int_0^1 (S(x') - x') \, dx' \right)^2 dx. \tag{24}$$

U varies with x_j more smoothly than D does, and its significance is $Q_{KS}(\pi p U)$ (Kendall and Stuart 1967). We will use U for testing the uniformity of R_j and C_j since it is practically more effective and robust than D to ensure a good matching over the whole N range.

For any given distribution f we compute a "best guess" for the "true" column densities by maximizing the product of the significances relative to U_R and to U_C (hereafter referred to as $\mathcal{L}_R$ and $\mathcal{L}_C$, respectively). There are always infinite guesses which allow a uniform distribution for R_j. However R_j and C_j are mutually dependent and their relationship depends on f (see Eqs. (20) and (21)). For an incorrect choice of f or of the estimated ranges $[N_{min,j}, N_{max,j}]$ it may then become impossible to derive uniform distributions for R_j and C_j at the same time.

4.3. Numerical results

Given an original distribution function for the face-on total column density of absorbers of the form:

$$g_\perp \left(N_{\mathrm{H}\perp}, z \right) = K (1+z)^\gamma N_{\mathrm{H}\perp}^{-\alpha} \tag{25}$$

and a functional relationship between $N_{\rm H\perp}$ and $N_{\rm HI\perp}$, a routine derives the Maximum Likelihood values of α and γ for an average absorber cross section $\hat{\sigma}$ (Eq. (7)). K is fixed by the normalization condition to the total number of detections (Eq. (17)); γ accounts both for cosmological effects, and for the physical evolution of the absorbers. Here we assume no evolution in the power-law index α in a given z interval and a pure power-law dependence for $g_\perp$, but it would be straightforward to implement our routine if necessary to change these assumptions. Physically meaningful $N_{\rm HI\perp}$–$N_{\rm H\perp}$ profiles in various redshift ranges have been computed by simulating the ionization structure of gaseous slabs (see Paper I). To identify each profile we use the parameter X defined as:

$$X = \lg_{10}\left(N_{\rm H\perp}/N_{\rm HI\perp}\right) \qquad \text{for} \quad N_{\rm HI} = 1.6\times10^{17}\,{\rm cm}^{-2}. \tag{26}$$

(the corresponding $N_{\rm HI\perp}$ depends on $\hat{\sigma}$). An increasing value of X corresponds to a neutral-to-ionized transition getting sharper and occurring at higher $N_{\rm H}$. After determining the best α for fixed values of the parameters X, γ and (h/R) we can determine the best values for these 3 parameters by comparing the relative Maximum Likelihood solutions. We use the Likelihood given in Eq. (19) with p_1 as the number of detections with an $N_{\rm HI}$ uncertainty, $\lg_{10} N_{max} - \lg_{10} N_{min} \leq \Delta\left(\lg_{10} N_{\rm HI}\right)$. Values for R_j and C_j are computed for all the remaining $(p-p_1)$ detections. Such a computation is not relevant for the Likelihood maximization itself, but it is useful in order to compare the theoretical and the observational cumulative. Since it is not always possible to obtain uniformly distributed R_j and C_j for any set of model parameters, the uniformity level of R_j and C_j distributions is a further test on the quality of the fit to $f(N_{\rm HI})$ distribution. For this reason the routine maximizes the product of $\mathcal{L}_R$ and $\mathcal{L}_C$.

The main results of our statistical fit procedure to data in the redshift range [1.75,3.25], where most of the observations are, have been discussed in Paper I, together with the relative cosmological implications. The Maximum Likelihood solution, $\alpha = 2.70$ and $X = 2.82$, is obtained for $\gamma = 1.0$ and $h/R = 0.2$ but α and X are only weakly sensitive to reasonable γ and h/R variations. We now investigate the possible dependence of α and of the cumulative function on the limiting value of $\Delta(\lg_{10} N_{\rm HI})$ for the treatment of errors, keeping X fixed to 2.82.

We consider 4 different cases: (a) no error treatment, i.e. for all absorbers we use the estimated HI column density (either the measured value or the middle point in the allowed $\lg_{10} N_{\rm HI}$ range); (b) and (c) error treatment has been applied to all the detections with $\Delta(\lg_{10} N_{\rm HI})$ equal to 0.9 and 0.5 respectively; (d) error treatment has been applied to all detections ($\Delta(\lg_{10} N_{\rm HI}) = 0$). Case (c) has been used for the results derived in Paper I. Fig. 3 shows the resulting value of α for the 4 cases and the comparison between the theoretical and observational cumulatives. Notice that, when the treatment of errors is operative, there

is a good match between the two cumulatives. The "observational" cumulatives in these cases (dotted histograms, in Fig. 3) depend on the assumed distribution, because the $N_{\rm HI}$ positions vary accordingly.

The logarithm of the Likelihood $\mathcal{L}_o$, normalized to its maximum value, is shown in Table 1 as we vary α for all the 4 cases. We can see that the maximum of the Likelihood is very well determined, without the presence of secondary maxima, and with 1-σ uncertainties of the order of 0.1. In Table 1 we also give the significances $\mathcal{L}_R$ and $\mathcal{L}_C$ of the uniformity of the R_j and C_j distributions. R_j and C_j can be uniformly distributed for a very wide range of α when the number of detections with variable $N_{\rm HI}$ is large; however only near the Maximum Likelihood value of α R_j and C_j are both uniformly distributed. The maximum of $\mathcal{L}_C$ is better defined than that of $\mathcal{L}_R$, and its position agrees more closely with that of the maximum value of $\mathcal{L}_o$. The uniformity of the C_j distribution represents a valid test of the goodness of the Maximum Likelihood solution and of the fitting routine.

In Paper I we have shown that, in the α-X plane, the constant-probability contours are elongated, giving a global uncertainty on α of about ± 0.3 when X uncertainties are taken into account. Fig. 4 shows the probability contours in the α-X plane for 3 redshift intervals which together cover all the redshifts in our compilation, each containing the same number of detections (~ 90). We find that at lower redshifts (Subsample A) the probability contours are shifted towards higher values of α and X; at higher redshifts (Subsample C) instead the allowed α values do not show significant changes, while X decreases. However, since these variations are of the same order of parameter uncertainties, they could just be statistical fluctuations. Further insight will come out from the simulated data analysis in the next session.

An issue that will be discussed more in detail in a future paper is whether line blending is present in the data and could affect the above results. The probability of blending of Lyman-α lines is relatively low for randomly distributed absorbers, but clustering or blending with some metal lines might imply a somewhat higher probability and affect lines with $5 \leq W < 10$ Å, sometimes declared as non damped. To address this point we have performed an analysis of the data without considering low-resolution searches for lines with $5 \leq W < 10$ Å: the α and X values that we find are consistent with those relative to the whole data sample. Therefore we tend to believe that our data sample closely reflects the real HI distribution.

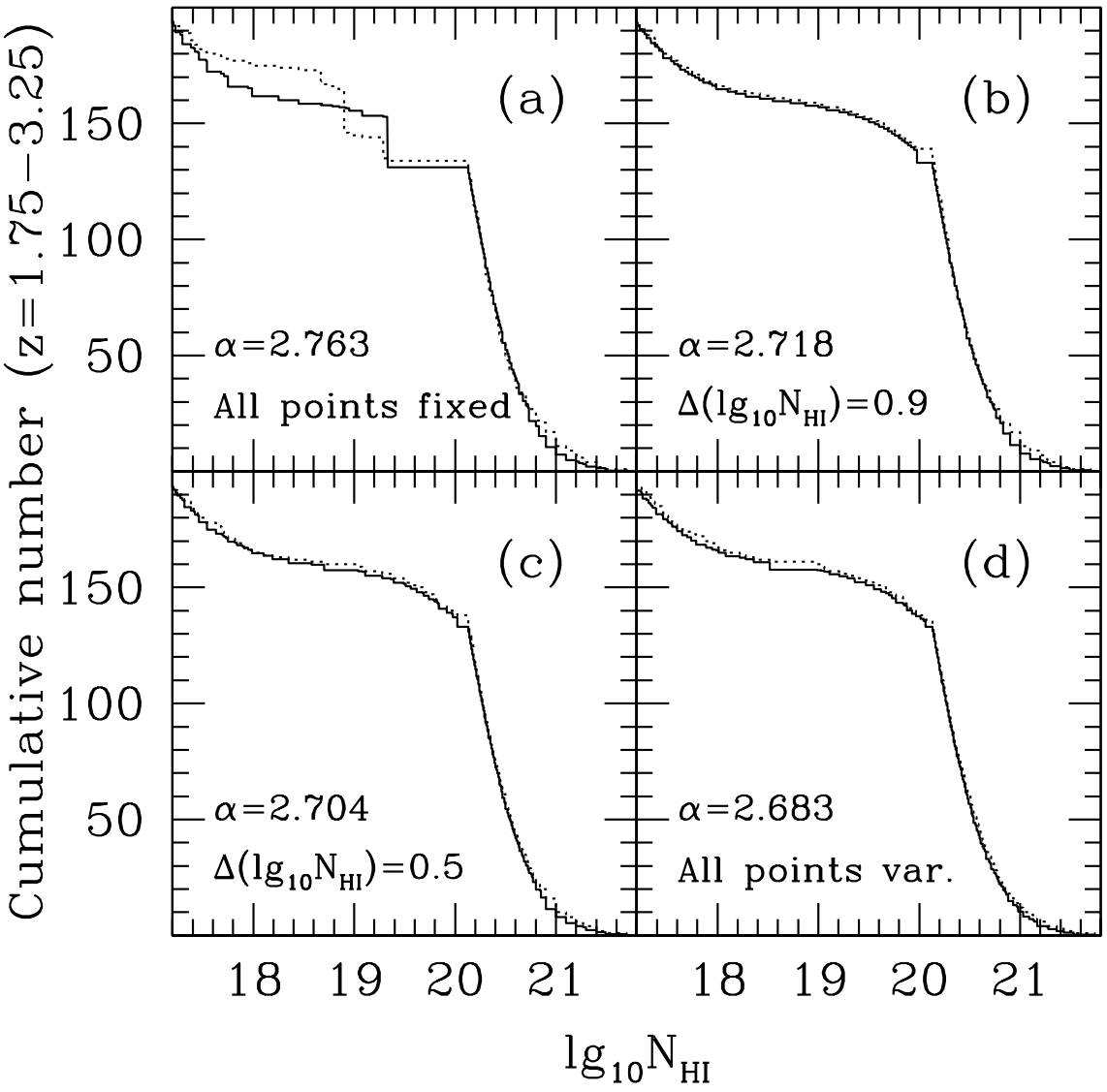

Fig. 3.— The Maximum Likelihood values of α and the corresponding cumulative number of absorbers in the z range [1.75,3.25] are shown for different prescriptions of the errors treatment. The solid line is the theoretical cumulative function, while the dotted line is the observational one.

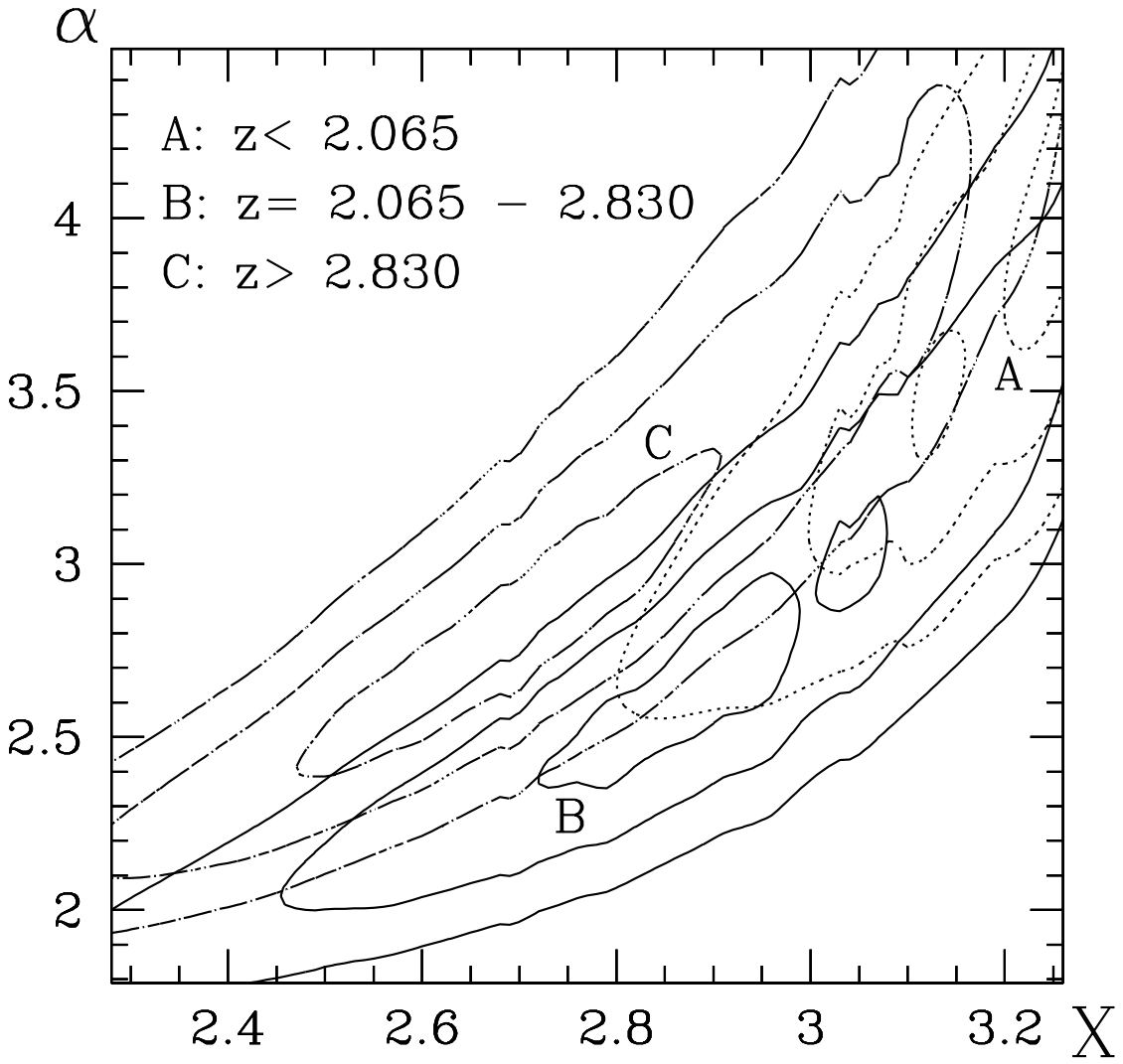

Fig. 4.— 1-σ, 2-σ and 3-σ confidence levels in the X-α plane, for 3 z-selected subsamples, labeled by A (dotted lines), B (solid lines) and C (dot-dashed lines).

5. Simulations

Possible biases might affect the data analysis, either related to our assumptions about the physical properties of the absorbers, or to our interpretation of the observations. In this section we show how to use simulated data for investigating the latter type of biases. These might derive from: *(i)* an uneven coverage of $N_{\rm HI}$ and z since the database contains results from surveys with different sensitivities; *(ii)* non uniform uncertainties in $N_{\rm HI}$; *(iii)* incorrect estimates of detection thresholds or of $N_{\rm HI}$ uncertainties. Simulated data can also be used to test the statistical procedure described in the previous section, and the confidence levels properties for the best fitting parameters.

5.1. The numerical procedure

Simulations supply, in a controlled way, a large number of samples to which we can apply our statistical analysis. We have devised a routine to simulate data in a highly realistic way: starting from an "a priori" distribution function for the absorbers total column densities, it generates a data set compatible with a given column density and redshift coverage. In the present work we use a coverage consistent with the observations listed in our database. The basic ingredients of the simulation are: 1. an original distribution function of $N_{\rm H\perp}$ for absorbers of a given geometrical shape; 2. an $N_{\rm H\perp}$–$N_{\rm HI\perp}$ relationship for each redshift bin; 3. a $N_{\rm HI}$–z coverage for the simulated survey. After the total face-on column density has been transformed into a line of sight HI value, we introduce measurement errors similar to those present in the actual survey compilation. These errors are simulated by deriving first the random quantities R_j, uniformly distributed, and then locating the uncertainties $[N_{{\rm HI},min,j}, N_{{\rm HI},max,j}]$ such that the position of "true" values $N_{\rm HI}$ corresponds to R_j. When $(\lg_{10} N_{{\rm HI},min,j} + \lg_{10} N_{{\rm HI},max,j})/2$, is above $10^{17.68}\,{\rm cm}^{-2}$ the absorption is considered as saturated. In this case, if there has been a search for the corresponding damped Lyman-α but the line has not been found, the uncertainty range is set to $[10^{17.68}, 10^{20.13}]\,{\rm cm}^{-2}$; if instead the damped Lyman-α line has not been searched for, the uncertainty range is set to $[10^{17.68}, 10^{21.7}]\,{\rm cm}^{-2}$.

For saturated absorption we simulate also the shadowing effect. Shadowed absorbers are eliminated from the sample and the $N_{\rm HI}$–z coverage of the survey is modified accordingly for LLS and DLS searches: this "after-shadowing" coverage is what should be compared with the real data coverage.

5.2. Simulation results

We first simulate samples of data consistent with the Maximum Likelihood solution $\alpha = 2.683$, $X = 2.82$, obtained for real data in the z range [1.75,3.25] for $p_1 = 0$. Results of the statistical analysis on one of our simulated data samples are shown in Fig. 5, where the efficiency of our method in recovering the original distribution is clear. Fig. 5 is the analogous of Fig. 3 for real data, the only difference being that now in (a) the "true" values of $N_{\rm HI}$ for simulated data are used, without any degradation by measurement processes and are compared directly with the model. The slight disagreement between the two curves in (a) is indicative of the magnitude of statistical fluctuations in the simulation.

$\mathcal{L}_o$, $\mathcal{L}_R$ and $\mathcal{L}_C$ for the simulated sample show a behavior very similar to that for real data (Table 1). An increase in the number of detections on which the treatment of errors is applied improves the match between the "measured" distributions and the original ones. Our algorithm is very efficient in recovering the original R_j distribution as well but there is no way to recover the original R_j values of individual detections. Detections with the same range of column densities are in all respects identical among themselves, and any permutation between their respective R_j values cannot be traced (i.e. there is no correlation between the "true" and derived R_j values).

To investigate if the selection of an error threshold affects the determination of α we have produced 5000 different simulated samples with $\alpha = 2.683$. On each sample we apply the analysis with the 4 different error thresholds as in Fig. 5. The results, reported in Table 2, show that the best fit α values are only slightly smaller than the original ones, and the dispersion for the best α values found ($\sigma(\alpha)$) is consistent with the average estimated uncertainty ($< \sigma >$).

We can also use the simulated data to check the uncertainties in the best-fitting parameters (α,X) by producing a confidence level map for the simulated data, for 3 z-selected subsamples, analogously to what has been done in Section 4.3 for the real data (Fig. 4). Fig. 6 shows for one simulated sample that the confidence levels present an elongation similar to the levels in Fig. 4. This means that in the real data there is no evidence of deviations of the gas distribution from our model assumptions. The elongation depends on a partial degeneracy of models in the α-X plane: α should increase as X increases to give the same slope for the distribution of low HI column density LLS, a drawback that will be difficult to cure by a moderate increase of the numbers of known absorbers.

By looking at the three subsamples (Fig. 6) it is clear that statistical fluctuations are present mostly in the direction of the elongation, consistently with the estimated uncertainties. With the present sample coverage the real data are still consistent with no evolution of

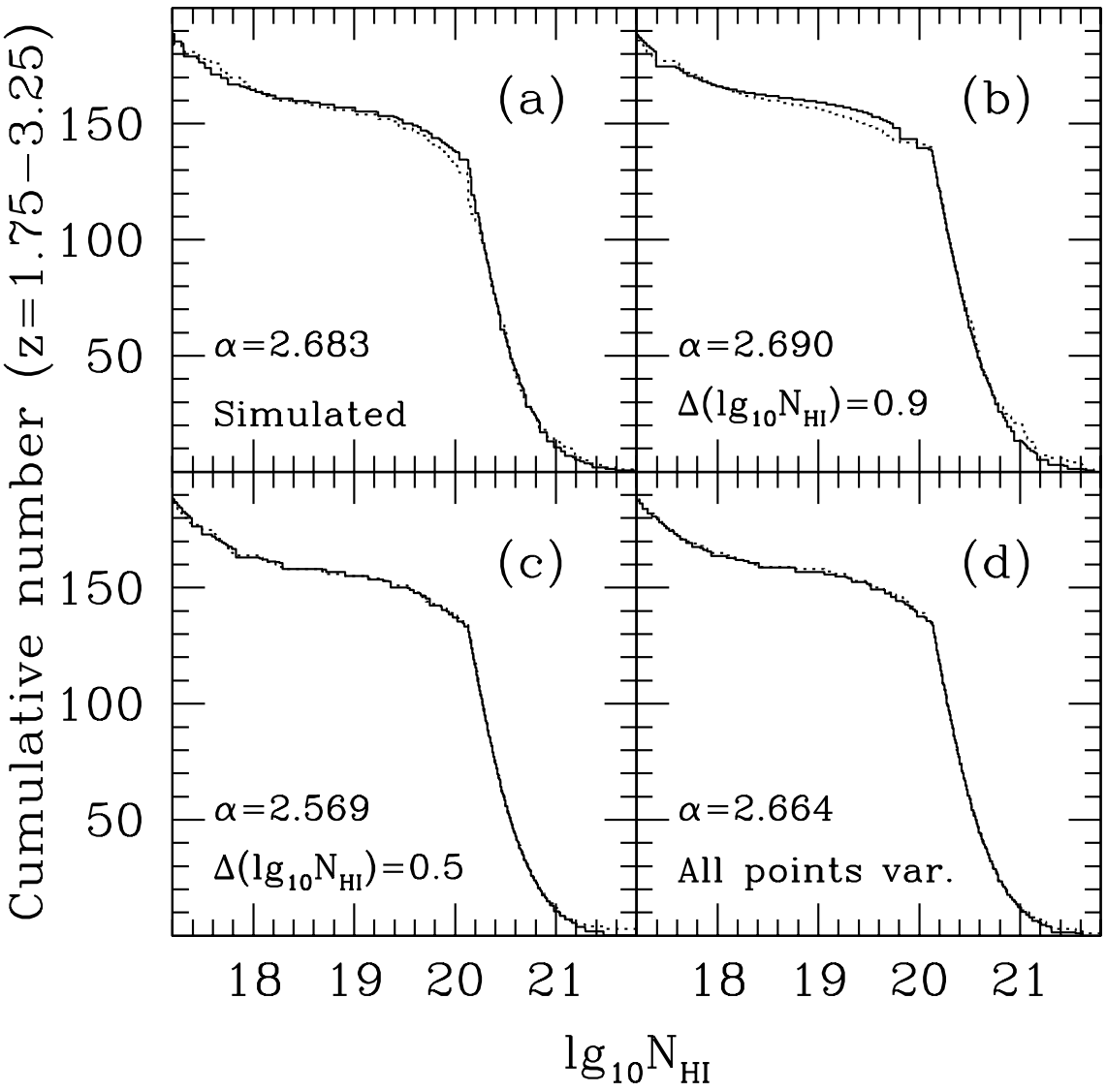

Fig. 5.— Various fits to the cumulative number of absorbers in the z range [1.75,3.25], on simulated data. This figure is analogous to Fig. 3, except for panel (a), which gives the "true" cumulative distributions, both theoretical (solid line) and "measured" (dotted line).

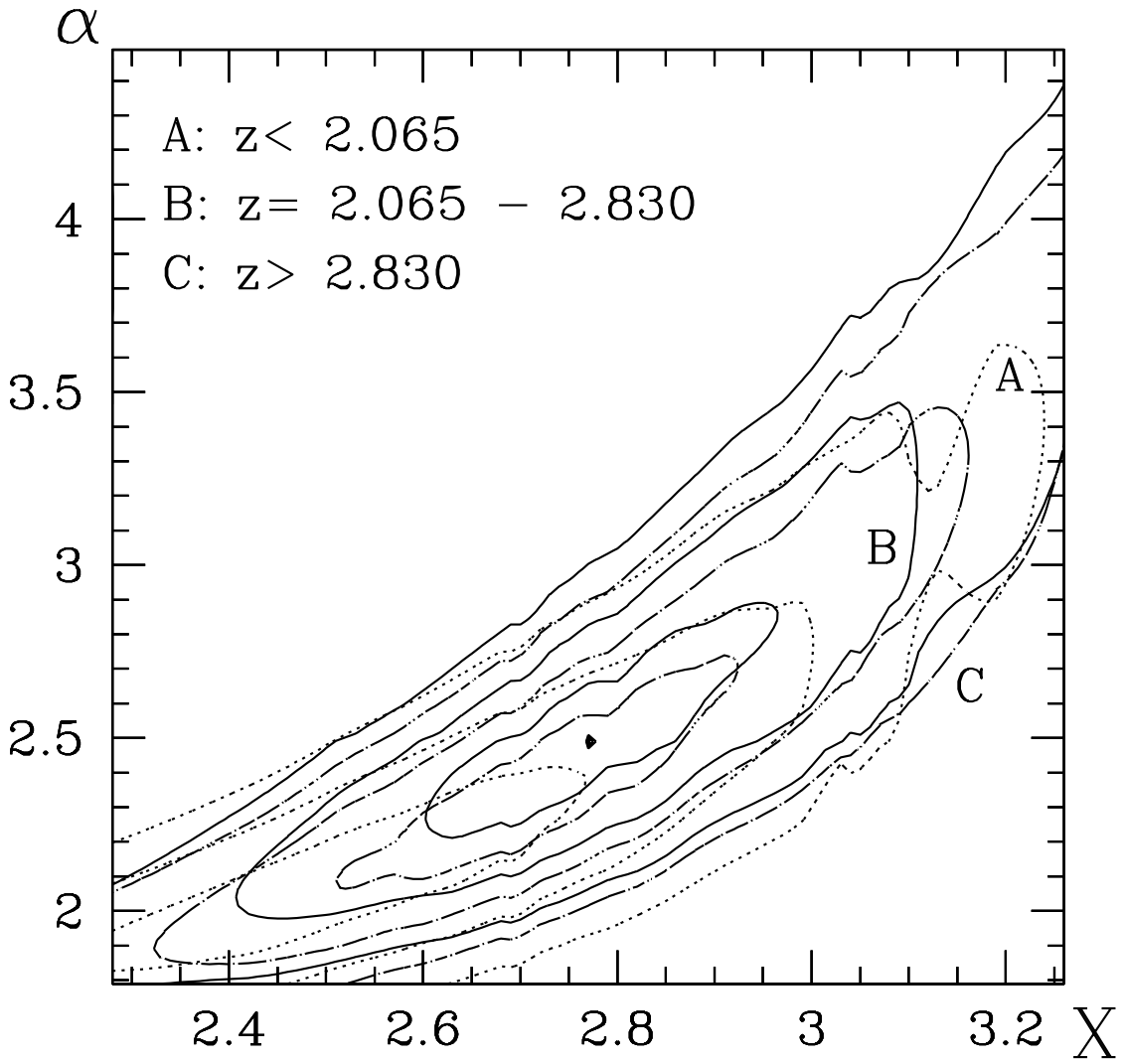

Fig. 6.— Map of the confidence level in the X-α plane, relative to a simulated sample, for 3 z-selected subsamples. All definitions in this figure are analogous to those in Fig. 4.

α and X, but some evolution cannot be excluded, especially for the high redshift sample. For this sample in fact the shift of the probability contours is not in the direction of elongation but mostly towards lower values of X. This would imply that either the ionizing flux is lower or that the absorbing gas has higher volume densities than at lower redshifts. Our analysis shows that in order to have a definite answer on the evolution of α and X closer contour levels are needed. This can be achieved by determining observationally the column density of saturated LLS (through lines in other spectral regions or through the recover of the quasar flux at shorter wavelengths) or by increasing the number of known high $N_{\rm HI}$ DLS.

REFERENCES

Aurière, M. 1982, A&A, 109, 301

Bahcall, J. N., Bergeron, J., Boksenberg, A., Hartig, G. F., Jannuzi, B. T., Kirhakos, S., Sargent, W. L. W., Savage, B. D., Schneider, D. P., Turnshek, D. A., Weymann, R. J., and Wolfe, A. M. 1993, ApJS, 87, 1

Bechtold, J., Green, R. F., Weymann, R. J., Schmidt, M., Estabrook, F. B., Scherman, R. D., Wahlquist, H. D., and Heckman, T. M. 1984, ApJ, 281, 76

Canizares, C. R., Grindlay, J. E., Hiltner, W. A., Liller, W., and McClintock, J. E. 1978, ApJ, 224, 39

Corbelli, E., Salpeter, E.E., and Bandiera, R. 2001, ApJ, 549, in press (Paper I)

Courvoisier, T. J.-L., and Paltani, S., eds. 1992, IUE-ULDA Access Guide No. 4A (ESA SP 1153)

Cristiani, S., D'Odorico, S., D'Odorico, V., Fontana, A., Giallongo, E., and Savaglio, S. 1997, MNRAS, 285, 209

Djorgovski, S., and King, I. R. 1984, ApJ, 277, L49

Hagiwara, K., and Zeppenfeld, D. 1986, Nucl.Phys., 274, 1

Harris, W. E., and van den Bergh, S. 1984, AJ, 89, 1816

Hénon, M. 1961, Ann.d'Ap., 24, 369

Jannuzi B. T., Bahcall, J. N., Bergeron, J., Boksenberg, A., Hartig, G. F., Kirhakos, S., Sargent, W. L. W., Savage, B. D., Schneider, D. P., Turnshek, D. A., Weymann, R. J., and Wolfe, A. M. 1998, ApJS, 118, 1

Kauffmann G. 1996, MNRAS, 281, 475

Kendall, M.G., and Stuart, A. 1969, "The Advanced Theory of Statistics" Vol. 2 (Griffin: London)

King, I. R. 1966, AJ, 71, 276

King, I. R. 1975, Dynamics of Stellar Systems, A. Hayli, Dordrecht: Reidel, 1975, 99

King, I. R., Hedemann, E., Hodge, S. M., and White, R. E. 1968, AJ, 73, 456

Kron, G. E., Hewitt, A. V., and Wasserman, L. H. 1984, PASP, 96, 198

Lanzetta, K. M. 1988, ApJ, 332, 96

Lanzetta, K. M. 1991, ApJ, 375, 1

Lanzetta, K. M., Wolfe, A. M., Turnshek, D. A., Lu, L., McMahon, R. G., and Hazard, C. 1991, ApJS, 77, 1

Lanzetta, K. M., Wolfe, A. M., and Turnshek, D. A. 1995, ApJ, 440, 435

Lynden-Bell, D., and Wood, R. 1968, MNRAS, 138, 495

Newell, E. B., and O'Neil, E. J. 1978, ApJS, 37, 27

Ortolani, S., Rosino, L., and Sandage, A. 1985, AJ, 90, 473

Peterson, C. J. 1976, AJ, 81, 617

Rauch, M. 1998, ARA&A, 36, 267

Sargent, W. L. W., Steidel, C. C., and Boksenberg, A. 1989, ApJS, 69, 703

Savaglio, S., Cristiani, S., D'Odorico, S., Fontana, A., Giallongo, E., and Molaro, P. 1997, A&A, 318, 347

Spitzer, L. 1985, Dynamics of Star Clusters, J. Goodman and P. Hut, Dordrecht: Reidel, 109

Stengler-Larrea, E. A., Boksenberg, A., Steidel, C. C., Sargent, W. L. W., Bahcall, J. N., Bergeron, J., Hartig, G. F., Jannuzi, B. T., Kirhakos, S., Savage, B. D., Schneider, D. P., Turnshek, D. A., and Weymann, R. J. 1995, ApJ, 444, 64

Storrie-Lombardi, L. J., McMahon, R. G., Irwin, M. J., and Hazard, C. 1994, ApJ, 427, L13

Storrie-Lombardi, L. J., McMahon, R. G., Irwin, M. J., and Hazard, C. 1996, ApJ, 468, 121

Storrie-Lombardi, L. J., Irwin, M. J., and McMahon, R. G. 1996, MNRAS, 282, 1330

Storrie-Lombardi, L. J., and Wolfe, A. M. 2000, ApJ, 543, 552

Turnshek, D. A., Wolfe, A. M., Lanzetta, K. M., Briggs, F. H., Cohen, R. D., Foltz, C. B., Smith, H. E., and Wilkes, B. J. 1989, ApJ, 344, 567

Tytler, D. 1982, Nature, 298, 427

Tytler, D. 1987, ApJ, 321, 49

Weinberg, D. H., Miralda-Escude, J., Hernquist, L., and Katz, N. 1997, ApJ, 490, 564

Wolfe, A. M., Turnshek, D. A., Smith, H. E., and Cohen, R. D. 1986, ApJS, 61, 249

Wolfe, A. M., Lanzetta, K. M., Foltz, C. B., and Chaffee, F. H. 1995, ApJ, 454, 698

This preprint was prepared with the AAS LaTeX macros v5.0.

A. Averaged cross section for homogeneous ellipsoids

In this Appendix we compute analytically the differential cross section for absorbers which can be modelled as axisymmetric ellipsoids of constant density. We use a cartesian coordinate system (x, y, z) in which z is parallel to the line of sight. The ellipsoid has a semi-minor axis h and semi-major axes R along the orthogonal directions. If its axis of symmetry is tilted along the y axis by an angle θ with respect to the line of sight, the surface of the ellipsoid is:

$$\left(\frac{\sin^2\theta}{h^2}+\frac{\cos^2\theta}{R^2}\right)x^2+2\sin\theta\cos\theta\left(\frac{1}{h^2}-\frac{1}{R^2}\right)xz+\left(\frac{\cos^2\theta}{h^2}+\frac{\sin^2\theta}{R^2}\right)z^2=1-\frac{y^2}{R^2}. \quad \text{(A1)}$$

The spatial extent of the ellipsoid in the z direction is 2ζ. Defining:

$$\xi^2\equiv\cos^2\theta+\sin^2\theta\frac{h^2}{R^2}, \quad \text{(A2)}$$

we can write:

$$\zeta^2=\frac{h^2}{\xi^2}\left(1-\frac{x^2}{\xi^2R^2}-\frac{y^2}{R^2}\right). \quad \text{(A3)}$$

The column density along the line of sight is $N_{\rm HI}=2n\zeta$. Since $\zeta\leq h/\xi$ the $N_{\rm HI}$ distribution for a fixed orientation presents an upper cut of $N_{\rm HI\perp}/\xi$ (where $N_{\rm HI\perp}=2nh$ is the maximum face-on column density).

The ellipsoid cross section for column densities larger than $N_{\rm HI}$ is:

$$\Sigma(N_{\rm HI})=\pi R^2\xi\left(1-\left(\frac{\xi N_{\rm HI}}{N_{\rm HI\perp}}\right)^2\right) \quad \text{(A4)}$$

which gives the differential cross section for one fixed orientation in space:

$$\sigma(N_{\rm HI},\mu)=\pi R^2\frac{\xi^3N_{\rm HI}}{2n^2h^2}, \quad \text{(A5)}$$

($\mu\equiv\cos\theta$) and an orientation-averaged cross section:

$$\hat{\sigma}(N_{\rm HI})=\pi R^2\int_0^1\frac{\xi^3N_{\rm HI}}{2n^2h^2}\,\Theta\left(N_{\rm HI\perp}-\xi N_{\rm HI}\right)\,d\mu. \quad \text{(A6)}$$

Introducing the variables:

$$w=\frac{R\xi}{h}=\sqrt{1+\left(\frac{R^2}{h^2}-1\right)\mu^2};\qquad W=\frac{R}{h}\min\left(1,\frac{N_{\rm HI\perp}}{N_{\rm HI}}\right), \quad \text{(A7)}$$

the average differential cross section for randomly oriented absorbers is:

$$\begin{aligned}\hat{\sigma}(N_{\rm HI}) &= \pi R^2 \frac{2h^3 N_{\rm HI}}{N_{\rm HI\perp}^2 R^3 \sqrt{R^2/h^2-1}} \int_1^W \frac{w^4}{\sqrt{w^2-1}}\, dw \\ &= \pi R^2 \frac{3h^4 N_{\rm HI}\left(W\left(1+\frac{2}{3}W^2\right)\sqrt{W^2-1}+\lg\left(W+\sqrt{W^2-1}\right)\right)}{N_{\rm HI\perp}^2 R^4 \sqrt{1-h^2/R^2}}. \end{aligned} \quad \text{(A8)}$$

For $N_{\rm HI} < 2nh$ the $\hat{\sigma}(N_{\rm HI})$ increases linearly with $N_{\rm HI}$ while it vanishes for $N_{\rm HI} > 2nR$. In the intermediate range the behavior of $\hat{\sigma}$ is more complex, but for $N_{\rm HI} \ll 2nR$, the following approximation holds:

$$\hat{\sigma}(N_{\rm HI}) = \frac{A N_{\rm HI\perp}^2}{N_{\rm HI}^3}\left(1+\mathcal{O}\left(\left(\frac{hN_{\rm HI}}{RN_{\rm HI\perp}}\right)^2\right)\right), \quad \text{(A9)}$$

where $A = \pi R^2/2\sqrt{1-h^2/R^2}$. Notice the similarity between Eq. (A9) and Eq. (6) for infinitely thin slabs. In Fig. 7 we compare the exact solution for the ellipsoids of various axial ratios h/R to the approximate formula we use in our routines (Eq. (7)).

Although $\hat{\sigma}$ depends on the detailed shape of the absorbers, the approximation by a $N_{\rm HI}^{-3}$ power law with an upper cutoff is appropriate for ellipsoids as well as for other geometrical shapes, especially for thickness $h/R \ll 1$. The average value of the projected column density is instead more geometry dependent. For ellipsoidal absorbers this is:

$$\begin{aligned}\hat{N}_{\rm HI} &= \frac{\int_0^{N_{\rm HI\perp} R/h} N_{\rm HI}\hat{\sigma}(N_{\rm HI})\, dN_{\rm HI}}{\int_0^{N_{\rm HI\perp} R/h} \hat{\sigma}(N_{\rm HI})\, dN_{\rm HI}} \\ &= \frac{4N_{\rm HI\perp} R\sqrt{R^2-h^2}}{3\left(R\sqrt{R^2-h^2}+h^2\ln\left(\left(R+\sqrt{R^2-h^2}\right)/h\right)\right)}. \end{aligned} \quad \text{(A10)}$$

For $h \ll R$, $\hat{N}_{\rm HI}$ approaches $4N_{\rm HI\perp}/3$. This result differs from that for a slab, for which:

$$\hat{N}_{\rm HI} = 2N_{\rm HI\perp}\left(1-h/R\right) \Big/ \left(1-h^2/R^2\right), \quad \text{(A11)}$$

whose limiting value is $\hat{N}_{\rm HI} = 2N_{\rm HI\perp}$ for infinitesimal thickness.

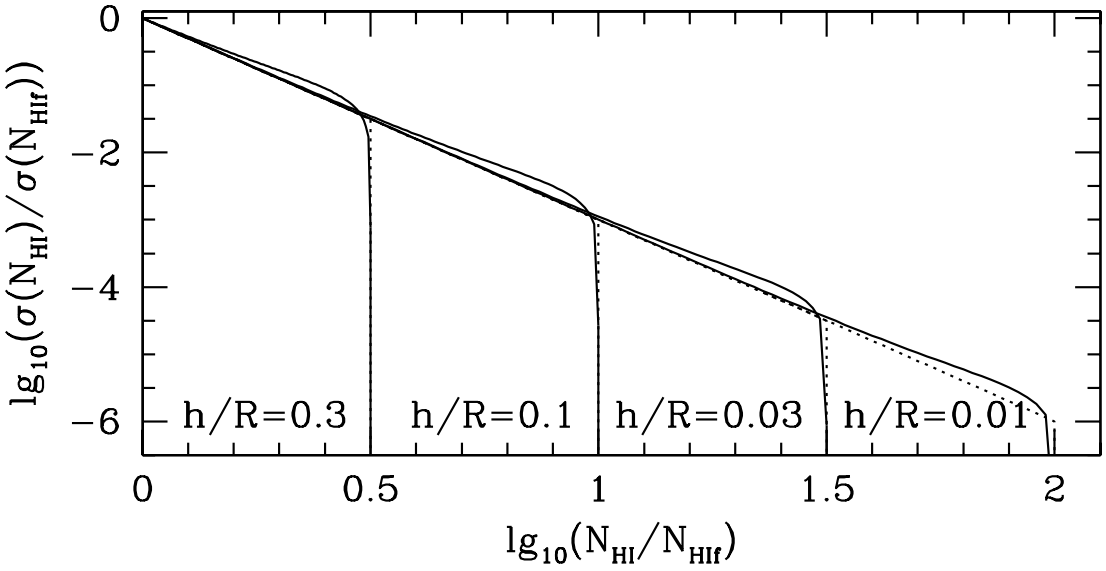

Fig. 7.— Comparison between orientation-averaged cross sections for ellipsoids (solid curves) and those for the finite slab approximation (dotted curves), for various axial ratios ($h/R = 0.3, 0.1, 0.03, 0.01$).

Table 1. Best fits to the data[a]

	Case (a)	Case (b)			Case (c)			Case (d)		
	All points fixed	$\Delta(\lg_{10} N_{\rm HI}) > 0.9$			$\Delta(\lg_{10} N_{\rm HI}) > 0.5$			All points var.		
α	$\ln \mathcal{L}_o$	$\ln \mathcal{L}_o$	$\ln \mathcal{L}_R$	$\ln \mathcal{L}_C$	$\ln \mathcal{L}_o$	$\ln \mathcal{L}_R$	$\ln \mathcal{L}_C$	$\ln \mathcal{L}_o$	$\ln \mathcal{L}_R$	$\ln \mathcal{L}_C$
2.05	–25.2	–21.5	–0.083	–6.218	–19.7	–0.022	–0.784	–18.1	0.000	0.000
2.15	–18.1	–15.0	–0.078	–3.784	–13.7	–0.014	–0.253	–12.4	0.000	0.000
2.25	–12.3	–9.91	–0.066	–1.999	–8.90	–0.003	–0.039	–7.94	0.000	0.000
2.35	–7.73	–5.94	–0.034	–0.939	–5.25	0.000	–0.001	–4.55	0.000	0.000
2.45	–4.31	–3.05	–0.011	–0.311	–2.61	0.000	0.000	–2.15	0.000	0.000
2.55	–1.93	–1.16	–0.002	–0.054	–0.92	0.000	0.000	–0.67	0.000	0.000
2.65	–0.52	–0.18	0.000	–0.006	–0.11	0.000	0.000	–0.03	0.000	0.000
2.75	0.00	–0.05	0.000	–0.003	–0.09	0.000	0.000	–0.18	0.000	0.000
2.85	–0.31	–0.71	0.000	–0.006	–0.82	0.000	0.000	–1.04	0.000	0.000
2.95	–1.39	–2.10	0.000	–0.025	–2.24	0.000	0.000	–2.57	0.000	0.000
3.05	–3.20	–4.18	0.000	–0.225	–4.31	0.000	0.000	–4.73	0.000	0.000
3.15	–5.68	–6.90	0.000	–0.851	–6.98	0.000	–0.015	–7.47	0.000	0.000
3.25	–8.80	–10.2	0.000	–1.857	–10.2	–0.002	–0.138	–10.8	0.000	–0.008
3.35	–12.5	–14.1	–0.000	–3.175	–14.0	–0.005	–0.476	–14.6	–0.001	–0.131
3.45	–16.8	–18.5	–0.001	–4.780	–18.3	–0.014	–1.067	–18.8	–0.005	–0.504
3.55	–21.6	–23.4	–0.001	–6.648	–23.0	–0.032	–1.929	–23.6	–0.010	–1.122

[a]Fits for $X = 2.82$, $h/R = 0.2$, $\gamma = 1.0$, $\lg_{10} N_{th} = 17.20$ and data in the redshift range [1.75,3.25].

Table 2. Results for 5000 simulations

Case	α	$\alpha - \alpha_{true}$	$\sigma(\alpha)$	$< \sigma >$
(a)	2.549	–0.134	0.116	0.106
(b)	2.468	–0.215	0.113	0.106
(c)	2.569	–0.114	0.122	0.116
(d)	2.554	–0.129	0.120	0.116